DOI: 10.1002/adma.200700237

Fabrication and Nanocompression Testing of Aligned Carbon-Nanotube–Polymer Nanocomposites**

By *Enrique J. García*,* *A. John Hart*, *Brian L. Wardle*, and *Alexander H. Slocum*

The exceptional electronic, thermal, and mechanical properties of carbon nanotubes (CNTs) have motivated extensive research on their manufacturing and applications. At bulk scales, there is particular interest in property enhancements by adding CNTs to polymers to make composite materials. Most work on CNT-based composites presented in the literature to date has focused on dispersion of single- or multi-walled CNTs (SWNTs or MWNTs) in the matrix; however, bulk CNTs embedded in a polymeric matrix tend to form aggregates that are not only poorly adhered to the matrix but also concentrate stresses, compromising the effect of the CNTs as reinforcement.[1] On the other hand, establishing order and alignment among CNTs within a composite matrix offers significant further potential to harness the properties of individual CNTs at bulk scales by realizing the anisotropic properties of CNTs in desired directions, and by enabling packing and dispersion of CNTs at much higher volume fractions than in tangled configurations.

In this work, CNT–polymer composites are manufactured by wetting as-grown arrays of vertically aligned CNTs rapidly and effectively (lack of voids) using off-the-shelf polymers. The wetting process not only preserves the alignment of the CNTs, but also allows the controlled manufacturing of nanocomposite test structures. Direct characterization of the mechanical properties of the nanocomposite structures is also presented in this work. The mechanical-reinforcement results support the feasibility of using these CNT arrays in large-scale hybrid advanced composite architectures reinforced with aligned CNTs. Such composites will also benefit from multifunctional property (e.g., electrical conductivity) enhancements owing to the aligned CNTs.

[*] Dr. E. J. García, Dr. A. J. Hart, Prof. B. L. Wardle, Prof. A. H. Slocum
Departments of Aeronautics and Astronautics and Mechanical Engineering
Massachusetts Institute of Technology
77 Massachusetts Avenue, Cambridge, MA 02139 (USA)
E-mail: ejgarcia@mit.edu

[**] Facilities of the MIT Technology Laboratory for Advanced Materials and Structures (TELAMS), Nanomechanical Technology Laboratory (Nanolab) Center for Material Science and Engineering (CMSE), and Microsystems Technology Laboratories (MTL) were used extensively in this work. E.J.G. is grateful for the support of a Fundación La Caixa Fellowship. A.J.H. is grateful for the support of a Fannie and John Hertz Foundation Fellowship. CNT growth facilities were operated with funding from NSF DMI-0521985. Supporting Information is available online from Wiley InterScience or from the author.

The mechanical properties (e.g., Young's modulus, hardness) of thin films containing randomly oriented CNTs inside a polymer matrix have been assessed using various techniques, that is, analytical models,[2–5] standard tension and compression tests,[6–10] and nanoindentation techniques.[11–15] The composite modulus along the CNT axis (stiff axis) of well-aligned CNT–polymer composites has not been studied to date. In the most relevant related work, Fang et al.[16] used Berkovich nanoindentation to determine the hardness of chemical vapor deposition (CVD)-grown aligned MWNT–parylene nanocomposites, but did not report their modulus. Parylene is a gas-phase deposited polymer typically used for electrical isolation. Modulus characterization in the transverse direction (i.e., CNTs aligned perpendicular to the direction of modulus measurement) indirectly inferred from structural tests was reported, with a significant increase (by a factor of 20–30) over the assumed modulus of parylene. Modulus characterization using direct measurement methods, not dependent on structural models, is preferred when available.

The present work is the first to characterize the mechanical properties of well-aligned CNT–epoxy nanocomposites along the CNT axis using direct measurement methods; this allows an assessment of the effectiveness of the CVD-grown CNT reinforcement by direct comparison to results obtained for non-reinforced polymers. Compression tests, obtained by using a diamond flat punch mounted on a nanoindenter, were used to acquire direct measurements of the load-displacement response of the aligned CNT–epoxy nanocomposites fabricated by using a submersion technique,[12,13] and compared directly to the measured modulus for pure epoxy pillars (identical test structure). Two grades of SU-8 UV-curing thermoset epoxy (Microchem 2000.1 and 2025)[17] were selected to create the nanocomposites. The direct measurement results show that Young's modulus increased from 3.7 GPa for the non-reinforced epoxy to 11.8 GPa for the vertically aligned CNT-reinforced composite material (220 % increase at 2 % volume loading). The mechanical properties of the pure polymer are the same for both grades; the CNT-reinforced pillars were manufactured with SU-8 2000.1.

SU-8 epoxy was selected for four main reasons: i) Because of its UV curing activation, it is possible to selectively cure 2D patterns to create 3D structures. SU-8 has been used in the fabrication of microfeatures such as microchannels, micromolds, and pure epoxy pillars similar to the ones used in this research; allowing the fabrication of test structures for direct comparison with the nanocomposites. ii) The surface of the pure SU-8 films or pillars is sufficiently regular to allow for

 © 2007 WILEY-VCH Verlag GmbH & Co. KGaA, Weinheim WILEY InterScience DISCOVER SOMETHING GREAT

ADVANCED MATERIALS

the nanocompression tests without additional surface treatment or polishing. iii) At room temperature, the viscosity of SU-8 is similar to the viscosity (during the curing stage) of thermosets typically used in the fabrication of advanced structural composites.[34] iv) As demonstrated by our prior work on wetting interactions between commercially available polymers and CNT arrays, this epoxy is the most effective matrix for the creation of regularly contracted, fully wet, vertically aligned nanocomposite pillars.[12,13, 35,36]

Microfabrication techniques were used to create pure SU-8 films and pillars for nanocompression tests using standard procedures including spin-coating, UV-curing, and pre/post-baking (see Experimental). A scanning electron microscopy (SEM) image of an epoxy pillar with a diameter of 40 μm and a height of 70 μm is shown in Figure 1a. The top surfaces of the pure SU-8 pillars are flat after curing, and do not need to be polished or microtomed prior the nanocompression tests.

Aligned CNT–SU-8 nanocomposite microstructures ("pillars") were created by CVD growth of CNTs followed by wetting with SU-8 using a submersion method.[12] First, cylindrical and aligned CNT pillars having a wide range of diameters were grown on a silicon wafer using a thermal CVD process.[18] The CNT pillars contained high-quality, regularly spaced (ca. 80 nm), and vertically aligned MWNTs with a diameter of 10 nm. The height of the tested CNT pillars (40–70 μm) was controlled by changing the time the wafer was exposed to the carbon source during the CVD process. The CNT pillars were subsequently wetted by SU-8 using the submersion method (see Experimental). The regularity of the contraction and the vertical alignment of the CNTs following wetting and curing are shown in Figure 1b and c. As seen in Figure 1d, a relatively small crown (ca. 5–7 μm tall) formed at the top of the pillar owing to contraction of the CNTs during wetting. The CNT–SU-8 pillars contain approximately 350 CNTs μm^{-2}, and the pillar cross sections vary from 490 μm^2 to 1300 μm^2.

As seen in Figure 1b and c not all of the cylindrical pillars contract regularly and remain vertical; however, both of these criteria must be met for nanocompression testing. SEM was used to identify the best pillars in terms of vertical alignment and regular contraction, and also to measure the dimensions of each individual pillar (height and surface area at the top of the pillar). Only pillars having sufficiently regular contraction as well as vertical alignment were compression-tested.

Because of the scale of the aligned CNTs, the mechanical characterization of the nanocomposites employed a nanoindenter for strain and displacement resolution. The nanocompression tests were performed using a Nanotest 600 nanomechanical testing system (Micro Materials, UK).[19] The nanoindenter monitors and records the load and displacement of the indenter with a force resolution of ca. 100 nN and a displacement resolution of about 0.1 nm.[20] By using a flattened diamond punch (conical diamond nanoindenter,[19] flattened using a focused ion beam to create a flat circular surface of 80 μm), compression tests were performed inside the thermally insulated environmental chamber of the nanoindenter at room temperature (25 ± 0.5) °C and at a relative humidity of 45 % ± 2 % on pure polymer and nanocomposite pillars. The compression test applied to nanocomposite pillars is illustrated in Figure 2. A compression test using a flattened punch mounted on a nanoindenter has been successfully used to mechanically characterize micrometer-scale metal pillars[21] as

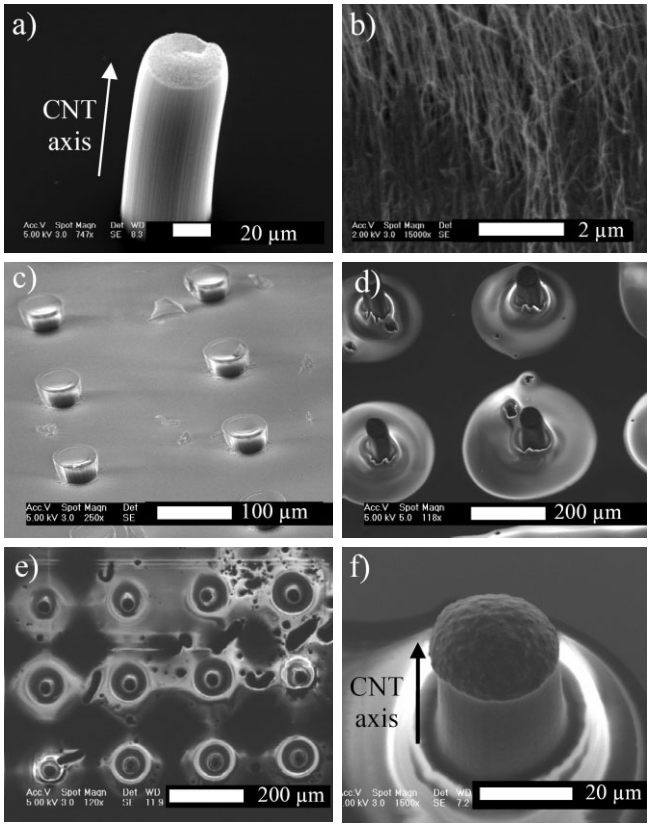

Figure 1. SEM images of a) a CNT pillar, showing the direction of the CNT axis; b) the alignment of the CNTs; c) a pattern of SU-8 pillars with a diameter of 40 μm, used in the nanocompression tests; d) an oblique (30°) view of aligned CNT–SU-8 nanocomposite pillars with relatively well-controlled contraction; e) a top-view of the same pillars; and f) an oblique (30°) view of a CNT–SU-8 pillar (note the crown formed during contraction) showing the regular contraction and the verticality of the pillar after wetting.

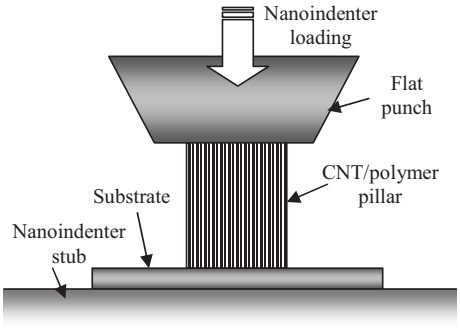

Figure 2. Illustration of compression test of an aligned CNT nanocomposite using a nanoindenter with a diamond flat punch.

© 2007 WILEY-VCH Verlag GmbH & Co. KGaA, Weinheim

well as the buckling of non-reinforced CNTs.[22] However, the use of this technique for characterizing aligned nanocomposites has not been previously reported.

The mechanical properties of an epoxy resin are highly dependent on the rate of testing.[23] Therefore, to be able to compare the results obtained for the non-reinforced epoxy matrix and the nanocomposites the test parameters were held constant. A complete description of standard nanoindentation experimental techniques has been reported by Bhushan and Li.[24,25] Thirty compression tests were applied on pure SU-8 pillars, and 25 compression tests were performed on the CNT–SU-8 nanocomposite pillars.

By using the dimensions measured by SEM before the compression tests, the load–displacement curves for each individual pillar were transformed into stress–strain curves to determine the Young modulus. The compression test using the nanoindenter was taken to be equivalent to a flat punch nanoindentation, and the unloading load-displacement curves were analyzed using Oliver–Pharr theory,[26–28] with the projected area for a compression test being the area of the pillar. This is referred to as projected area in typical nanoindentation analyses. The moduli of the pure SU-8 pillars measured from loading ((3.9 ± 0.1) GPa) and unloading ((3.7 ± 0.3) GPa) analysis are in excellent agreement (5.5 % higher in loading; Fig. 3).

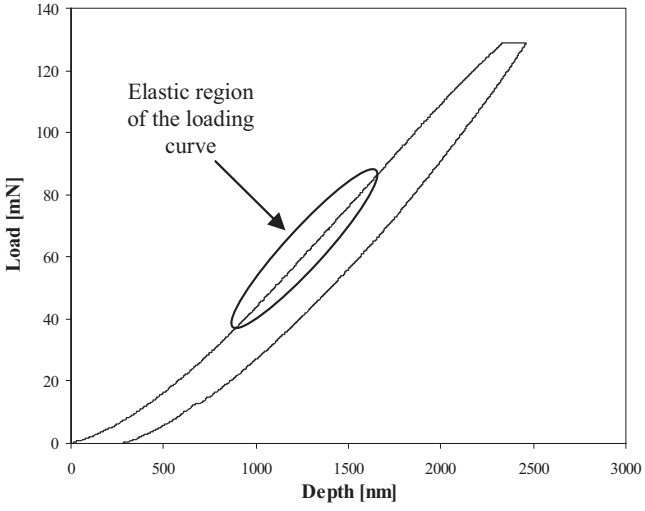

Figure 3. Representative load–depth curve for a compression test on a non-reinforced SU-8 pillar.

Of the 25 nanocomposite pillars selected for testing by SEM, 19 specimens did not produce pure compression tests, and the results obtained from those tests were discarded (see Supporting Information). The remaining 6 pillars, however, allowed pure compression tests, and these results were used to evaluate the composite reinforcement. SEM images of one of the pillars subjected to pure compression tests before and after the test are shown in Figure 4. As seen in Figure 4a and b, the alignment and regularity of the contraction during wetting are excellent. Also, it is important to note that the pillars had a small region of CNTs on top, forming a dome with a height of ca. 5–7 μm for pillars with total lengths in the range of 40–70 μm.

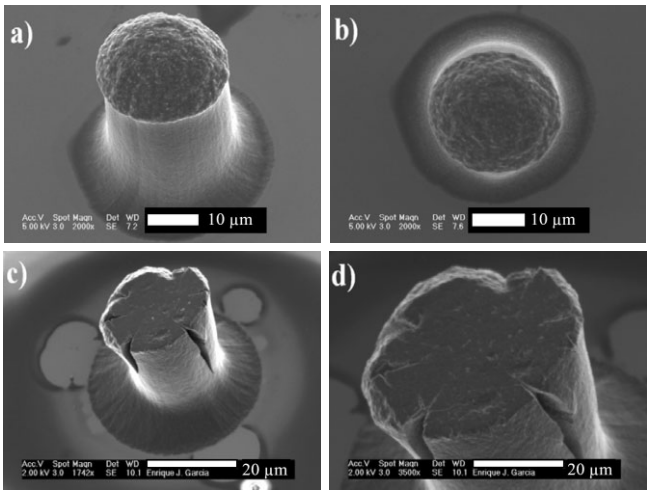

Figure 4. SEM images (30° inclination) of a) a vertical CNT–SU-8 nanocomposite pillar; b) a top-view of the pillar, showing verticality and regular contraction; c) a pillar after compression test (note that the dome has been flattened out during the test); and d) a closer view of the flattened dome.

During the compression test, this dome was flattened by the punch, as can be seen in Figure 4c and d. Also noteworthy was the formation of vertical cracks between the aligned CNTs (see Fig. 4c and d) during the compression test in all six specimens.

A typical load–depth curve obtained from the 6 compression tests is shown in Figure 5, corresponding to the pillar shown in Figure 4. The initial phase of the test flattened the dome, as indicated by the stiffening response in Figure 5. The cracks shown in Figure 4c and d are believed to be formed at

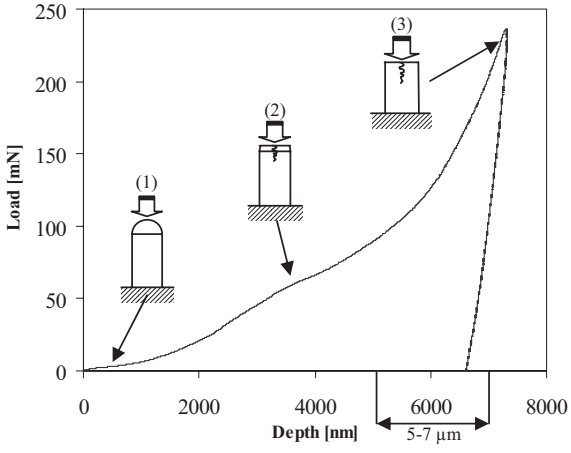

Figure 5. Representative load–depth curve for pure compression tests. The illustration shows the initial phase where the dome is flattened (1), the formation of transverse cracks (2), and a change in slope as the CNT–SU-8 nanocomposite below the dome takes the load (3).

 © 2007 WILEY-VCH Verlag GmbH & Co. KGaA, Weinheim

ADVANCED MATERIALS

the region of the load–depth curve marked as (2), which corresponds to a mild softening of the nanocomposite pillar (decrease of the slope of the curve). After the dome was flattened, the slope of the load–depth curve increases considerably, evidencing the stiffness resulting from reinforcement of the SU-8 flat pillar with aligned CNTs.

The load–depth curves for the pure compression tests show that because of the presence of the dome, there is no linear-elastic region that can be analyzed to determine the elastic modulus during loading. Owing to limitations on the deflection range in the nanoindenter, further compression beyond ca 7 μm was not possible. However, the Oliver–Pharr indentation technique can be used to analyze the unloading region, which was shown earlier to be in good agreement with elastic loading for the SU-8 pillars. The results obtained from the unloading analysis of the compression tests applied to non-reinforced SU-8 and CNT–SU-8 pillars are compared in Table 1. The effective reinforcement for these pillars is close to 220 %, increasing the Young's modulus on average from 3.7 to 12 GPa. Also, it is important to note that the standard deviation for these pillars (1.409 GPa) is larger than the results obtained for non-reinforced SU-8 owing to the reduced number (six) of tests available.

Table 1. Comparison of the Young's modulus of non-reinforced SU-8 and CNT–SU-8 pillars obtained from compression tests.

	Unreinforced SU-8	CNT/SU-8 Nanocomposite	Reinforcement
Young's modulus [GPa]	3.69 ± 0.31	11.82 ± 1.41	220 %

Because of the contraction of the CNT–SU-8 pillars during wetting, the volume fraction of CNTs increased from the original value of 0.9 % to ca. 2 %. The original volume fraction was calculated considering a spacing between the MWNTs of 80 nm and the CNTs as solid tubes with an inner diameter of 5 nm and an outer diameter of 10 nm. A previous study achieved a comparable modulus enhancement by using a 5 % volume fraction of randomly oriented SWNTs.[11] This is in agreement with the atomistic models developed by Odegard et al.,[2] which showed that the reinforcement is three times more effective when the nanotubes are oriented in the direction of the load. The Young's modulus reinforcement of the SU-8 in this work using aligned CNTs is compared to previous results of thermoset polymeric matrices reinforced with unaligned CNTs[29] in Figure 6. Note that the effective reinforcement using randomly oriented CNTs decreases with higher volume fractions owing to the creation of CNT agglomerates. The vertically aligned architecture presented in this work overcomes that limitation.

It is interesting to contrast the results obtained in this work with a simplified "rule-of-mixtures" model of the nanocomposite. Assuming perfect alignment of the CNTs, perfect wetting of the CNTs by the epoxy, perfect bonding in the interface between the CNTs and the epoxy, perfect bonding between the concentric tubes of a MWNT, and matrix properties unchanged by the addition of CNTs, a simplified rule of mixtures predicts:

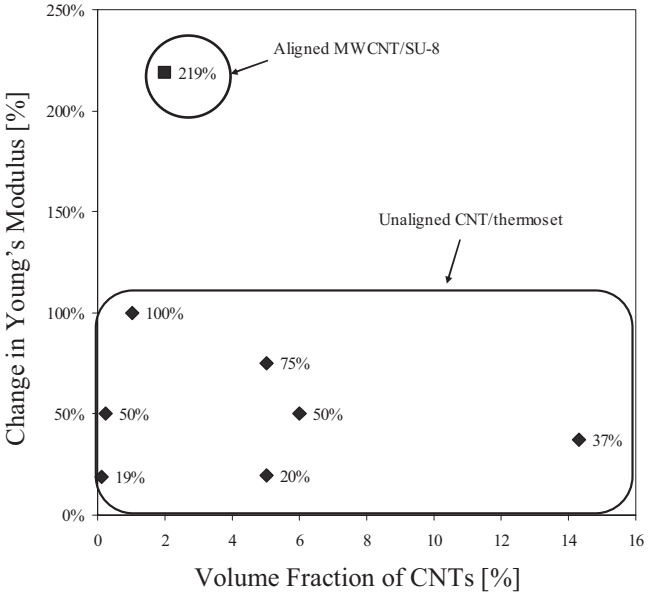

Figure 6. Change in moduli of CNT-reinforced thermoset polymers reinforced with unaligned single- or multiwalled CNTs (◆) [29], and the results from this work (■).

$$E_{\text{nanocomp}} = E_{\text{CNT}} V_{\text{CNT}} + E_{\text{matrix}}(1 - V_{\text{CNT}}) \quad (1)$$

where E_{nanocomp}, E_{CNT}, and E_{matrix} are, , the Young's modulus of the nanocomposite, the modulus of pure CNTs (assumed to be 1 TPa for this simplified calculation), and the modulus of the non-reinforced SU-8 (3.7 GPa as shown in Table 1), respectively, and V_{CNT} is the volume fraction of CNTs (ca. 2 %). A separate modulus calculation, considering that the void inside the MWNT was not filled by the polymer, differed 0.01 % from the result calculated here without considering the voids. Equation 1 treats the MWNT as a solid tube, and therefore E_{CNT} will be much lower than the CNT wall modulus.[30]. The ideal Young's modulus for the CNT–SU-8 nanocomposite, calculated using the rule of mixtures presented in Equation 1, is 23.6 GPa, two times larger than the 11.8 GPa obtained from the compression tests. The difference between the theoretical reinforcement and the one obtained in the nanocompression tests may be explained by assumptions in the simplified model: the CNTs in the nanocomposite are self-aligned, not vertically aligned in a perfect manner; the bonding between the CNTs and the polymer matrix is not perfect, though it has been shown to be strong;[30–32] the bonding between the tubes in a MWNT is also not perfect, as shown in the sword–sheath experiments reported elsewhere;[33] and/or the CNT modulus is closer to 0.5 TPa than to 1.0 GPa. Taking these factors into account, the measured modulus increase owing to the CNTs indicates that the aligned CNT–thermoset pillars

 © 2007 WILEY-VCH Verlag GmbH & Co. KGaA, Weinheim

behave like a typical aligned-fiber composite. This is indirect, but excellent, evidence of good wetting and strong bonding of the CNTs to the polymer, and of the high Young's modulus of the CNTs themselves.

In conclusion, the feasibility of hybrid composite materials strongly depends on the two factors studied experimentally in this work: wetting of the carbon nanotubes with thermoset polymers and effective reinforcement of the matrix by the CNTs. The wetting results show that the capillarity effect wets CNTs with polymers having viscosities similar to resins used as matrices for traditional composite materials. More importantly, direct measurements for the Young's modulus of aligned CNT–polymer nanocomposites along the CNT axis using nanocompression tests show that the addition of well-aligned CNTs to a polymer matrix effectively reinforces the matrix, as in typical composite materials. The effective reinforcement obtained for the CNT–epoxy nanocomposites tested in this work is below that predicted by the idealized rule of mixtures, but considerably higher than that reported by previous work using randomly oriented CNTs embedded into a polymer matrix.

These initial results demonstrate the feasibility of fabricating hybrid composite architectures based on reinforcing traditional advanced fiber–polymer composites with aligned arrays of CNTs grown by using the thermal CVD method. Future studies will address nanocompression tests using a nanoindenter embedded into an SEM with a higher displacement range for both direct modulus and strength measurements, and will test arrays with a higher volume fraction of CNTs to assess the scalability of wetting and reinforcement. The feasibility of the hybrid composite fabrication process[37,38] will be investigated through wetting and mechanical characterization tests of fiber cloths and prepreg (preimpregnated) laminates covered with CNTs.

Experimental

Substrate Preparation: The substrates were clean 6″ (100)-oriented silicon wafers (Silicon Quest International). A catalyst film of 1/10 nm Fe/Al_2O_3 was deposited by electron-beam evaporation in a single pump-down cycle using a Temescal VES-2550 instrument with a FDC-8000 film-deposition controller. Catalyst patterns were fabricated by lift-off of a 1 μm layer of image-reversal photoresist (AZ-5214E): The photoresist was patterned by photolithography, catalyst was deposited over the entire wafer surface, and subsequently the catalyst areas on the photoresist were removed by soaking in acetone for 5 min with mild sonication.

Carbon Nanotube Growth Procedure: CNT growth was performed in a single-zone atmospheric pressure quartz tube furnace (Lindberg) having an inside diameter of 22 mm and a heating zone 30 cm long, using flows of Ar (99.999 %, Airgas), C_2H_4 (99.5 %, Airgas), and H_2 (99.999 %, BOC). The substrate sample was rested in the furnace tube at a starting location 40 mm downstream of the control thermocouple. The furnace temperature was ramped to the set point in 30 min, and held for an additional 15 min under 400 sccm Ar. The Ar and H_2 flows used during growth were established 5 min prior to introducing C_2H_4, after which time the 100:500:200 sccm $C_2H_4/H_2/Ar$ mixture was maintained for the growth period of 1.5 min. Finally, the H_2 and C_2H_4 flows were discontinued, and 400 sccm Ar was maintained for an additional 10 min to displace the reactant gases from the tube, before being reduced to a gentle stream while the furnace cooled to below 100 °C.

Pure SU-8 Microstructure Fabrication Procedure: Microchem SU-8 2025 and low-viscosity SU-8 2000.1 (1.25 cPs) were used to fabricate non-reinforced (SU-8 2025) and CNT-reinforced (SU-8 2000.1) microstructures (films and pillars) using microfabrication techniques. A 2 mL drop of SU-8 2025 was placed on a previously cleaned Si wafer. Spin-coating (Headway spinner) the wafer at 1000 rpm for 45 s resulted in a 40 μm layer of SU-8. The wafer was then prebaked at 65 °C for 2 min, and at 95 °C for 5 min, using standard hot plates (following the SU-8 standard process). A Karl Suss MJB3 mask aligner with a previously fabricated mask was used to selectively expose the wafer to UV light ($\lambda = 320$ nm) for 1.5 min and cure a regular pattern of cylindrical pillars with a diameter of 40 μm. The wafer was post-baked at 65 °C for 1 min and at 95 °C for 3 min to minimize residual stresses resulting from the curing process. A further post-baking step was performed at 135 °C for 24 h.

Wetting of the CNT Microstructures Procedure: Details about the submersion method used to wet the vertically aligned CNT microstructures have been previously published [12]. The substrate with CNT pillars was inverted on a stage above a reservoir containing the SU-8 resin (Microchem SU-8 2000.1). The substrate was then lowered until the pillars contacted the surface of the reservoir. The CNT pillars were soaked for 2 min, and subsequently the SU-8 was cured by the standard process: prebaking at 65 °C for 2 min and at 95 °C for 5 min using standard hot plates, UV curing (using a Karl Suss MJB3 with no mask) for 90 s, postbaking 1 min at 65 °C and 3 min at 95 °C, and a final post-baking step at 135 °C for 24 h.

Nanocompression Test Procedure: A typical nanocompression experiment consisted of four subsequent steps: approaching the surface, loading to peak load, holding the indenter at peak load for 60 to 120 s depending on the material of the specimen, and finally unloading completely. Initial tests were used to determine acceptable test parameters for the compression tests: maximum load and depth (7 μm) and, more importantly, the load rate (1 $mN\,s^{-1}$), and the time hold at the maximum load (60 to 120 s) to avoid creep effects in the results. A series of four indents were performed on three different specimens for each material. A summary of the tests performed to mechanically characterize the aligned CNT-reinforced nanocomposites is presented in Table 2.

Table 2. Test matrix of mechanical nanocomposite tests.

Set of tests	Type of test	Material	Specimen	Number of tests
2	Compression	SU-8	Pillars (40 μm high)	30
3	Compression	CNT/SU-8	Pillars (40-70 μm high)	25[a]

[a] Nineteen of these tests failed to create a state of uniaxial compression, and the CNT–polymer pillars fractured in a bending mode as described in the Supporting Information.

Characterization: Scanning electron microscopy (SEM) was performed by using a FEI/Philips XL30 FEG SEM field-emission high-resolution microscope operating at 5 kV.

Received: January 27, 2007
Revised: March 8, 2007
Published online: July 12, 2007

[1] E. T. Thostenson, Z. Reng, T. Chou, *Compos. Sci. Technol.* **2001**, *61*, 1899.

[2] G. M. Odegard, T. S. Gates, K. E. Wise, C. Park, E. J. Siochi, *Compos. Sci. Technol.* **2003**, *63*, 1671.

 © 2007 WILEY-VCH Verlag GmbH & Co. KGaA, Weinheim

[3] G. M. Odegard, S. J. V. Frankland, T. S. Gates, *AIAA J.* **2005**, *43*, 1828.
[4] F. T. Fisher, R. D. Bradshaw, L. C. Brinson, *Appl. Phys. Lett.* **2005**, *80*, 4647.
[5] S. Frankland, A. Caglar, D. W. Brenner, M. Griebel, presented at the MRS Fall Meeting 2000, Boston, MA, November 2000.
[6] A. Star, J. F. Stoddart, D. Steuerman, M. Diehl, A. Boukai, E. W. Wong, *Angew. Chem. Int. Ed.* **2001**, *40*, 1721.
[7] A. Dufresne, M. Paillet, J. L. Putaux, R. Canet, F. Carmona, P. Delhaes, *J. Mater. Sci.* **2002**, *37*, 3915.
[8] A. Miravete, P. Laborde-Lahoz, W. Maser, T. Martínez, A. Benito, T. Seeger, P. Cano, R. Guzmán de Villoria, *Mech. Adv. Mater. Struct.* **2005**, *12*, 1.
[9] M. C. Paiva, B. Zhou, K. A. S. Fernando, Y. Lin, J. M. Kennedy, Y.-P. Sun, *Carbon* **2004**, *42*, 2849.
[10] F. H. Gojny, M. H. G. Wichmann, U. Köpke, B. Fiedler, K. Schulte, *Compos. Sci. Technol.* **2004**, *64*, 2363.
[11] X. Li, H. Gao, W. A. Scrivens, D. Fei, X. Xu, M. A. Sutton, A. P. Reynolds, M. L. Myrick, *Nanotechnology* **2004**, *15*, 1416.
[12] E. J. Garcia, *M. Sc. Thesis*, MIT (Cambridge, MA) **2006**, Ch. 3.
[13] E. J. García, A. J. Hart, B. L. Wardle, A. H. Slocum, *Nanotechnology* **2007**, *18*, 165 602.
[14] A. K. Dutta, D. Penumadu, B. Files, *J. Mater. Res.* **2004**, *19*, 158.
[15] M. Olek, K. Kempa, S. Jurga, M. Giersigm, in *Tech. Proc. of the 2005 NSTI Nanotechnology Conf. and Trade Show* **2005**, *2*, 167.
[16] W. Fang, H.-Y. Chu, W.-K. Hsu, T.-W. Cheng, N.-H. Tai, *Adv. Mater.* **2005**, *17*, 2987.
[17] http://www.microchem.com/products/pdf/SU8_2002-2025.pdf (accessed June 2007).
[18] A. J. Hart, A. H. Slocum, *J. Phys. Chem. B* **2006**, *110*, 8250.
[19] http://www.micromaterials.co.uk/ (accessed June 2007).
[20] A. C. Fischer-Cripps, *Nanoindentation*, Mechanical Engineering Series, Springer, Berlin **2004**.
[21] J. R. Greer, W. D. Nix, *Appl. Phys. A* **2005**, *80*, 1625.
[22] J. F. Waters, L. Riester, M. Jouzi, P. R. Guduru, J. M. Xu, *Appl. Phys. Lett.* **2004**, *85*, 1787.
[23] http://gltrs.grc.nasa.gov/reports/2005/TM-2005-213595.pdf (accessed June 2007).
[24] X. Li, B. Bhushan, *Mater. Charact.* **2002**, *48*, 11.
[25] B. Bhushan, X. Li, *Int. Mater. Rev.* **2003**, *48*, 125.
[26] W. C. Oliver, G. M. Pharr, *J. Mater. Res.* **2003**, *18*, 1564.
[27] M. F. Doerner, W. D. Nix, *J. Mater. Res.* **1986**, *1*, 601.
[28] W. C. Oliver, G. M. Pharr, *J. Mater. Res.* **2004**, *19*, 3.
[29] J. N. Coleman, U. Khan, W. J. Blau, Y. K. Gun'ko, *Carbon* **2006**, *44*, 1624.
[30] H. J. Qi, K. B. K. Teo, K. K. S. Lau, M. C. Boyce, W. I. Milne, J. Robertson, K. K. Gleason, *J. Mech. Phys. Solids* **2003**, *51*, 2213.
[31] X. Xu, M. M. Thwe, C. Shearwood, K. Liao, *Appl. Phys. Lett.* **2002**, *81*, 2833.
[32] D. Qian, E. C. Dickey, R. Andrews, T. Rantell, *Appl. Phys. Lett.* **2000**, *76*, 2868.
[33] M. F. Yu, O. Lourie, M. Dyer, K. Moloni, T. Kelly, *Science* **2000**, *287*, 637.
[34] http://www.hexcel.com/NR/rdonlyres/B9DAF85C-DFA5-4158-8CE5-22A8F7146A94/0/HexFlowRTM6.pdf (accessed June 2007).
[35] E. T. Thostenson, C. Li, T.-W. Chou, *Compos. Sci. Technol.* **2005**, *65*, 491.
[36] E. J. García, A. J. Hart, B. L. Wardle, A. H. Slocum, presented at the Proc. of 47th AIAA/ASME/ASCE/AHS/ASC Structures, Structural Dynamics, and Materials Conf., Newport, RI 2005, AIAA-2006-1854.
[37] E. J. García, *Ph.D. Thesis*, Universidad de Zaragoza **2006**, Ch. 4.
[38] http://web.mit.edu/edu/aeroastro/www/people/wardle/documents/MTL_ar2006_WARDLE%201.pdf (accessed June 2007).

 © 2007 WILEY-VCH Verlag GmbH & Co. KGaA, Weinheim